RESEARCH ARTICLE

Photoactive antibodies enable light-mediated cell-specific transport of small molecules on the cell surface

Thomas Bridge[a], Saher A. Shaikh[a], Paul Thomas[b], Joaquin Botta[c], Peter J. McCormick[c] & Amit Sachdeva[a]*

Abstract: Antibodies have found applications in several fields, including, medicine, diagnostics, and nanotechnology; yet methods to modulate antibody-antigen binding using an external agent remain limited. We have developed photoactive antibody fragments by genetic site-specific replacement of single tyrosine residues with photocaged tyrosine, in an antibody fragment, 7D12. A simple and robust whole cell ELISA-based approach is developed to evaluate the light-mediated binding of 7D12 mutants to its target, epidermal growth factor receptor (EGFR), on the surface of cancer cells. Presence of photocaged tyrosine reduces 7D12-EGFR binding affinity by over 20-fold in two out of three 7D12 mutants studied, and binding is restored upon exposure to 365 nm light. Molecular dynamics simulations explain the difference in effect of photocaging on 7D12-EGFR interaction among the mutants. Finally, we demonstrate the application of photoactive antibodies in delivering fluorophores to EGFR-positive live cancer cells in a light-dependent manner.

Introduction

Chemists and biochemists have successfully designed molecular systems that can be controlled in a defined manner in response to external agents, such as pH, light, and small molecules.[1] Controlling the activity of small molecules and biomolecules has allowed development of molecular machines, novel drugs, and nano-delivery systems, that have found widespread applications.[2] Monoclonal antibodies are arguably one of the most versatile biomolecules that can be evolved to bind to different substrates with high selectively and specificity. Due to these properties, antibodies have found applications as building blocks in molecular electronics, as agents for detection of substrates in medical diagnosis and biotechnology, and as inhibitors of biological processes in biotherapeutics.[3]

Modulating antibody-antigen binding presents an opportunity to gain user-defined control over antibody-mediated processes. Despite immense potential, there are only a few reports on controlling the binding of antibodies to their target. Notable examples are, antibodies activated by tumor-specific proteases, and those activated by phosphatases. The former are generated by extending the N-terminal domain of the antibody, and are currently under investigation for cancer therapy.[4] The latter, antibodies activated by phosphatases, have been generated by chemically attaching phosphate at a specific site in an antibody fragment.[5] Both these approaches are dependent on addition of the activating enzyme, as well as the requirements that the N-terminal extension, or phosphate, effectively inhibit binding, while their removal restores binding despite the mutations introduced to add these groups to the antibody. Light-dependent activation, with site-specifically installed light-sensitive groups on the antibody, would present the opportunity to gain spatial and temporal control over antigen-antibody binding in a facile manner, independent of other molecules.

Selective therapeutic targeting of cells is a major challenge in medicine, particularly in cancer therapy. Light-activated small molecule cytotoxic drugs are currently under investigation for treatment of cancer, that could target cells in a localized area. [6] However, after photoactivation these drugs are often not cell-selective, and could cause side effects. Many antibodies and antibody-drug conjugates (ADCs) are in use, or in clinical trials, for treatment of cancer.[7] These antibodies exert cytotoxicity by binding and blocking the function of receptors on the surface of cancer cells, and in the case of ADCs, also delivering cytotoxic drugs to cancer cells. As the same cell surface receptors are often present on healthy cells, therapeutic antibodies can have severe side effects.[8] To partly address this challenge, antibodies linked to light-activated small molecule drugs have also been developed.[9] However, the antibody would still be able to bind to healthy cells independent of light. Controlling the direct binding of antibody to its corresponding antigen using light, at the site of cancer cells, can thus minimize the side effects of antibody-based therapeutics.

Over the last two decades, genetic code expansion has enabled site-specific incorporation of unnatural amino acids, including amino acids containing bioorthogonal functional groups, photoreactive amino acids and photocaged amino acids, into proteins. Photocaged amino acids, in particular, have been employed to control the activity of several biomolecules including DNA polymerase,[1d] RNA polymerase,[10] kinases,[11] proteases[12] and inteins[13], which have undoubtedly advanced our understanding of key biological processes. To the best of our knowledge, site-specifically incorporated photocaged amino acids have not been used to control the activity of therapeutic proteins, such as antibodies. In the present study, we show that modifying a single amino acid in the antigen binding region of an antibody fragment, 7D12, to its photocaged counterpart, inhibits its binding to its target, epidermal growth factor receptor (EGFR). EGFR is overexpressed in several cancers, including colorectal cancer, lung cancer, and head and neck cancer. Antibodies that bind to the extracellular domain of EGFR, block its downstream signaling

[a] Thomas Bridge, Dr. Saher A. Shaikh, Dr. Amit Sachdeva
School of Chemistry
University of East Anglia
Norwich-NR4 7TJ, United Kingdom
E-mail: a.sachdeva@uea.ac.uk
[b] Dr. Paul Thomas
The Henry Wellcome Laboratory of Cell Imaging
University of East Anglia
Norwich-NR4 7TJ, United Kingdom
[c] Dr. Joaquin Botta, Dr. Peter J. McCormick
Centre of Endocrinology, William Harvey Research Institute
Queen Mary University London
Charterhouse Square, London- EC1M 6BQ, United Kingdom

Supporting information for this article is given via a link at the end of the document.

and inhibit cell growth, [14] however, these cause severe side effects.[15] 7D12 belongs to a class of single domain antibody fragments isolated from camelids that have gained importance due to their small size and deep tissue penetration.[16] 7D12 has shown promise in treatment of cancers in mice model.[17]

Here, we demonstrate efficient genetic site-specific incorporation of photocaged tyrosine (**pcY**) into 7D12, generating photoactive antibodies. Using an on-cell assay, we show that the presence of a photocaging group at specific tyrosine residues in the antigen binding region of 7D12 inhibits its binding to EGFR on the surface of cancer cells and the binding is restored upon irradiation with 365 nm light. In order to explain why the binding of 7D12 to EGFR is affected by **pcY** at only certain positions at the binding interface, we investigated the 7D12-EGFR interaction using molecular dynamics (MD) simulations. Finally, we show that photoactive antibodies can mediate delivery of small molecule fluorophores to the surface of EGFR-positive live cancer cells.

Results and Discussion

Efficient genetic site-specific incorporation of photocaged tyrosine into antibody fragments. Wild-type 7D12 (wt7D12) was cloned into pSANG10 plasmid[18] forming pSANG10_7D12 plasmid (Supporting Information); pSANG10 has earlier been employed for efficient expression of single chain antibody fragments in the periplasm of *E. coli*.[18] Using pSANG10_7D12, we obtained a yield of 10.1 mg of wt7D12 per liter of culture after purification (Figure S2).

To design photoactive mutants of 7D12, we aimed to replace tyrosine residues in the antigen binding site of 7D12, **pcY**. Mutants of *Methanococcus jannaschii* Tyrosyl-tRNA synthetase (*Mj*RS)/MjtRNA pair and *Methanosarcina* Pyrrolysyl-tRNA synthetase (PylRS)/tRNA pair have been employed to genetically encode **pcY**.[19] Also, several suppressor plasmids have been used for unnatural amino acid incorporation in *E. coli*.[20] These plasmids contain orthogonal aminoacyl-tRNA synthetase (aaRS)/tRNA pairs that incorporate unnatural amino acids in response to an amber stop codon. These suppressor plasmids vary in their origin of replication, promotors that drive the expression of aaRS and tRNA, and the copy number of aaRS and tRNA genes. In order to find an optimal plasmid system and an aaRS/tRNA pair for incorporation of **pcY** in 7D12, we screened five suppressor plasmids containing either *Mj*CNFRS/*Mj*tRNA$_{CUA}$ pair (*Mj*CNFRS is an *Mj*RS evolved for incorporation of 4-cyano-L-phenylalanine) or the PylRS/tRNA$_{CUA}$ pair (Supporting information and Figure S3). pULTRA plasmid with *Mj*CNFRS/*Mj*tRNA$_{CUA}$ pair, and, pCDF plasmid with PylRS/tRNA$_{CUA}$ pair were most efficient at genetic incorporation of unnatural amino acids. Due to ease of cloning, we selected pULTRA plasmid and the *Mj*CNFRS/*Mj*tRNA$_{CUA}$ pair, replacing the *Mj*CNFRS with *Mj*pcYRS (aaRS evolved for pcY) for incorporation of **pcY** in 7D12 (Supporting Information).

Upon examining the crystal structure of 7D12 bound to domain III of EGFR (PDB ID: 4KRL),[21] we identified three tyrosine residues in the antigen binding site of 7D12, viz. Y32, Y109 and Y113, as candidates for developing photocaged mutants (Figure 1A). Y32, Y109 and Y113, were replaced with **pcY** by assigning amber stop codon, TAG, to these positions, forming the mutants, 7D12pcY32, 7D12pcY109, and 7D12pcY113, respectively. wt7D12 and the three amber mutants were expressed using cells containing the plasmid, pULTRA_*Mj*pcYRS/*Mj*tRNA$_{CUA}$, that directs site-specific incorporation of **pcY** in response to TAG codon, and the plasmids, pSANG10_7D12, pSANG10_7D12-32TAG, pSANG10_7D12-109TAG, or pSANG10_7D12-113TAG, that provide the gene for periplasmic expression of 7D12 and its amber mutants. Protein expression was performed both in the presence and absence of **pcY**. For the amber mutants, expression of full-length protein only occurred on addition of **pcY** (Figure 1B). Electrospray ionization mass spectrometry (ESI-MS) analysis of full-length 7D12 and the mutants was consistent with incorporation of **pcY** (Figure S2). The yield of 7D12pcY32, 7D12pcY109, and 7D12pcY113 after purification were 5.3, 3.2, 1.7 mg per litre of culture, respectively.

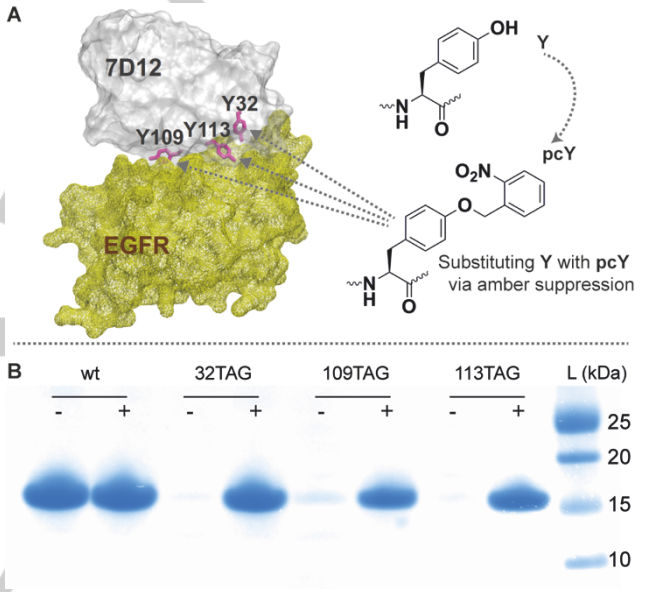

Figure 1. Genetic site-specific incorporation of **pcY** in 7D12. (A) Crystal structure of 7D12 (grey)-EGFR domain III (yellow) complex (PDB ID: 4KRL)[21] showing Y32, Y109, and Y113 (pink) in the antigen binding pocket of 7D12 that were replaced with **pcY**. (B) The expression of three amber mutants of 7D12, viz. 32TAG, 109TAG and 113TAG only occurs in the presence of **pcY**. Comparison of band intensities for amber mutants with wt7D12 shows efficient incorporation of **pcY**.

Assessing the binding of photoactive antibodies to EGFR on the surface of cancer cells. To study 7D12-EGFR binding, we adopted an assay that would report on this interaction in a cellular environment where other cell surface antigens are also present. For this purpose, A431 cells were used; these are human epidermal carcinoma cells with high levels of EGFR on their cell surface, and have been used in previous studies to validate EGFR targeting anti-cancer drugs.[17b, 22] In our on-cell assay, 7D12 and its mutants were incubated with live A431 cells, in media containing serum, thus allowing the binding to occur under physiologically relevant conditions. Following this, unbound 7D12 was removed, cells were fixed to the surface of the 96-well plate used, and the bound 7D12 was assessed via its C-terminus hexa-histidine tag (Figure 2A, Supporting information). Unlike several

other techniques used for measuring protein-protein interaction, this approach does not require sophisticated instrumentation or purified EGFR, and assesses the binding of antibody to EGFR on a cell surface. The technique is similar to whole cell enzyme-linked immunosorbent assay (ELISA) or on-cell western blots used for quantification of cell surface antigens.[23] A series of control experiments were performed to demonstrate the viability of the on-cell assay used in this study. When 7D12 was incubated with MDA-MB231,[22] a cell line with low levels of EGFR, the chemiluminescence signal was significantly lower compared to the signal for A431 cancer cell line (Figure S8). This supports our premise that the observed chemiluminescence is due to specific interaction between 7D12 and EGFR, and not due to non-specific binding of 7D12 to the cell surface. We also measured the binding of an unrelated His6-tagged antibody fragment, RR6-VHH,[24] to A431 cells using this assay. Near-background level of chemiluminescence was observed with RR6-VHH, demonstrating that the observed signal is not due to the non-specific interaction

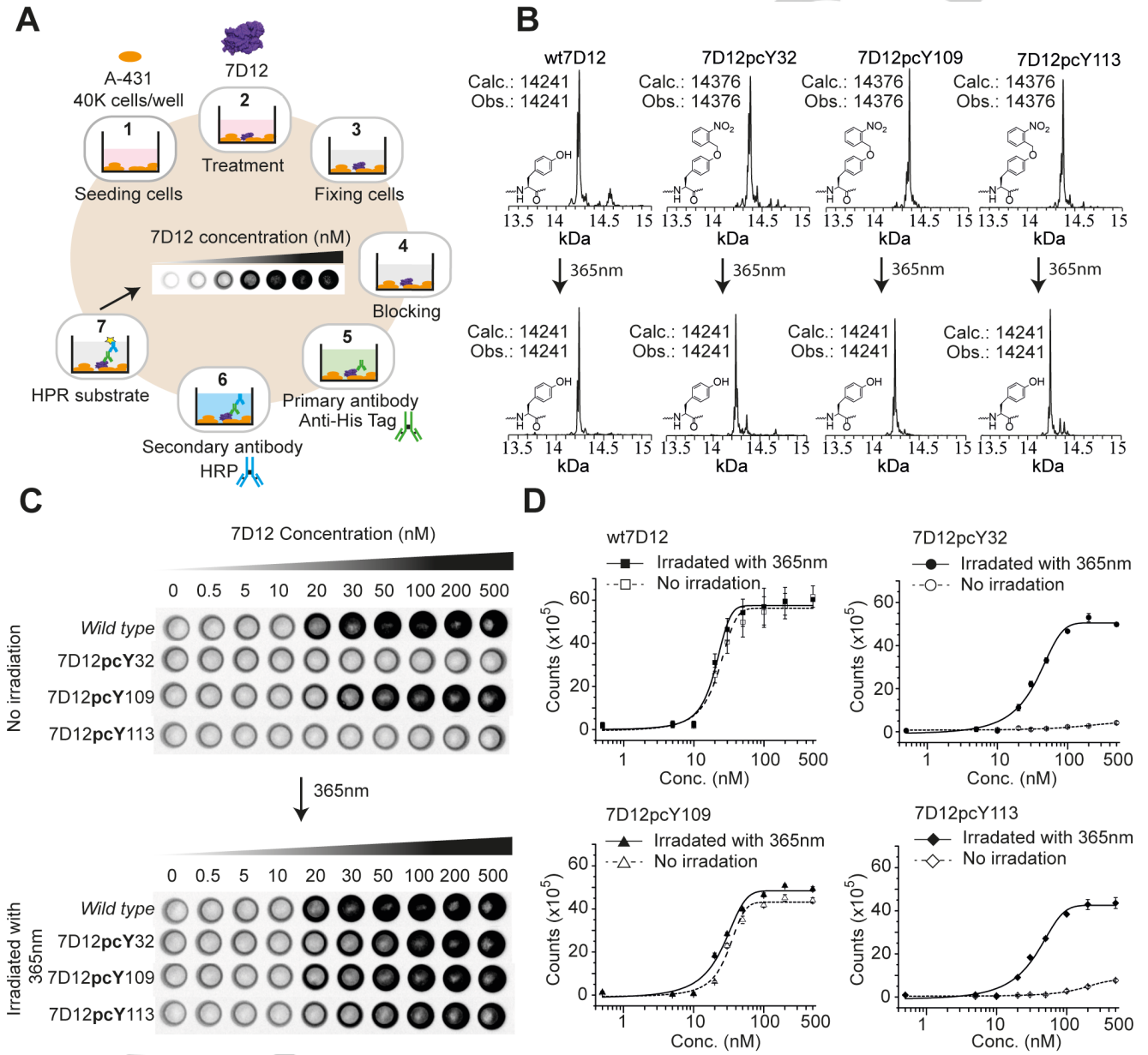

Figure 2. Assessing the binding of photocaged mutants of antibody fragment to EGFR on cell surface. (A) Schematic representation of procedure followed for measurement of 7D12-EGFR binding on the surface of A431 cancer cells. 1. 40,000 cells were seeded into each well of a 96-well plate. 2. These cells were incubated with the complete media containing the antibody fragment. 3. The antibody solution was replaced with 3.7% formaldehyde solution for fixing the cells. 4. This was followed by incubation with blocking solution. 5. Incubation with primary antibody specific for hexa-histidine tag. 6. incubation with HRP-linked secondary antibody. 7. The substrate for HRP was added and the cells were imaged for chemiluminescence (Supporting information). (B) Comparison of ESI-MS of photocaged mutants of 7D12 before and after irradiation with 365 nm light confirms light-mediated decaging. (C) On-cell binding assay demonstrates that the presence of pcY at positions 32 and 113 in 7D12 inhibits its binding to EGFR. However, 7D12pcY109 mutant shows binding affinity similar to wt7D12. The binding to 7D12pcY32 and 7D12pcY113 mutants is restored upon irradiation with 365 nm light. These experiments were performed in triplicate (Figure S7). (D) Chemiluminescence intensity was quantified using a CLARIOstar plate reader and plotted against log(concentration) of 7D12; the data fitted to sigmoidal nonlinear curve using ORIGIN curve fitting software (Supporting information and Figure S6).

of antibody fragments with A431 cancer cells (Figure S9). Prior to measuring the binding of photocaged mutants of 7D12 before and after decaging, we used ESI-MS to confirm light-mediated decaging of 7D12pcY32, 7D12pcY109, and 7D12pcY113. The molecular weight of all the pcY mutants was reduced to that of wt7D12 after irradiation with 365 nm light for 4 min, confirming the loss of o-nitrobenzyl group from tyrosine residues in the photocaged mutants (Figure 2B).

In order to assess if the presence of **pcY** at positions 32, 109 and 113 in 7D12, inhibits 7D12-EGFR binding, cell ELISA-based experiments were performed on the surface of A431 cells as described above. For wt7D12, as the concentration was increased from 0 to 100 nM, we observe an increase in chemiluminescence, followed by saturation of signal at higher concentrations. For the 7D12pcY32 and 7D12pcY113 mutants, near background chemiluminescence signal was observed even up to 500 nM concentration (Figure 2C), demonstrating that the binding between 7D12 and EGFR is inhibited due to the presence of **pcY** at positions 32 and 113 in 7D12. The binding of these mutants was recovered upon irradiation with 365 nm light; demonstrating light-mediated activation of antibody-antigen binding. Interestingly, **pcY** at position 109, despite being at the binding interface, does not inhibit 7D12-EGFR binding. We explain these differences in the binding affinity of photocaged mutants using MD simulations, later in this study.

We estimated the binding affinity of 7D12 to EGFR on the surface of A431 cells from the measured chemiluminescence signal. The log (concentration) was plotted against the chemiluminescence intensity and the curves were fitted to a sigmoidal function (Figure 2D, Supporting information). Based on these curve fittings, the K_D value of wt7D12 and 7D12pcY109 before irradiation with 365 nm light were estimated to be 22 (±2.4) nM and 30 (±4.6) nM respectively. The small increase in the K_D value of 7D12pcY109 mutant is presumably due to presence of **pcY**. For 7D12pcY32 and 7D12pcY113, near background level chemiluminescence was observed till 500 nM concentration, thus the K_D value is greater than 500 nM. After irradiation with 365 nm, the K_D values for wt7D12, 7D12pcY32, 7D12pcY109, and 7D12pcY113 were estimated to be 20 (±1.4) nM, 28 (±8.1) nM, 24 (±2.3) nM and 27 (±10.6) nM respectively. The estimated K_D value of caged mutants after irradiation with 365 nm light is close to wt7D12 indicating recovery of binding after photo-decaging.

Molecular dynamics simulations explain the difference in effect of pcY on the 7D12- EGFR interaction among mutants. In the crystal structure of 7D12-EGFR domain III complex (PDB ID: 4KRL), Y32, Y109, and Y113 residues in 7D12 lie at the binding interface. Hence, in our experiments, we expected that substituting any of these tyrosine residues with **pcY** could inhibit or affect 7D12-EGFR binding. While two of the mutants show expected behavior, i.e., significantly reduced binding to EGFR, the third mutant binds to EGFR with affinity comparable to wt7D12. We investigated this difference in binding behaviour through a description of 7D12-EGFR interactions and dynamics in the presence and absence of photocaging group, using MD simulations.

All-atom MD simulations were performed for four systems, starting from the 7D12-EGFR domain III crystal structure (PDB ID: 4KRL)[21] for wt7D12, and with **pcY** substitutions in mutants, 7D12pcY32, 7D12pcY109, and 7D12pcY113, respectively, in the presence of explicit water and ions, using NAMD 2.12 (Supporting Information).[25] Comparing the dynamics of the systems during 300ns simulations each, it is seen that wt7D12 and 7D12pcY109 remain bound to EGFR, while 7D12pcY32 and 7D12pcY113 show unbinding from EGFR for prolonged periods (Figure 3A). The root mean square deviation (RMSD) of the complex from the starting conformation (Figure 3B) shows a larger extent of movement in 7D12pcY32 and 7D12pcY113 compared to wt7D12 and 7D12pcY109 -visual analysis as well as measuring the number of contacts maintained by 7D12 with EGFR (Supporting information) confirms that this is due to frequent unbinding of

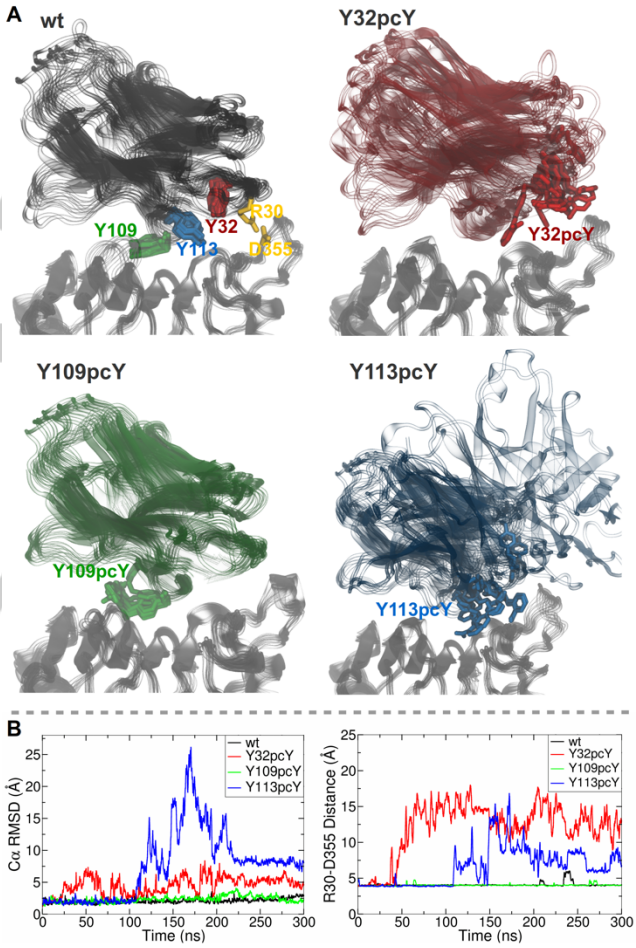

Figure 3. MD simulations of wt7D12 and three amber mutants (7D12pcY32, 7D12pcY109, and 7D12pcY113) show that wt7D12 and 7D12pcY109 form more stable complexes with EGFR domain III as compared to 7D12pcY32 and 7D12pcY113. (A) Simulation snapshots taken at intervals of 30 ns during 300ns simulations for each system, (EGFR- grey for all, wt7D12 - black, 7D12pcY32 - red, 7D12pcY109 - green, 7D12pcY113 - blue) highlight the extent of motion of 7D12. (B) Left: Root mean square deviations (RMSDs) from starting structure for protein Cα atoms during simulations. Right: The R30-D355 salt-bridge (residues shown in (A) wt7D12 snapshot, in yellow), monitored as the distance between the R30 guanidine C and the D355 carboxyl C, breaks frequently in the 7D12pcY32 and 7D12pcY113 systems. These observations suggest that the presence of pcY at positions 32 and 113 destabilizes the 7D12-EGFR domain III complex.

7D12 in the former two systems. Furthermore, a salt bridge formed by R30 in 7D12, and D355 in EGFR, described in previous experimental studies to play a key role in 7D12-EGFR binding,[21] shows frequent breakage in 7D12pcY32 and 7D12pcY113, while remaining stable in the wt7D12 and 7D12pcY109 systems. Looking closely at the 7D12-EGFR interface, it is seen from the wt7D12-EGFR simulations that Y32 and Y113, both form some non-specific interactions with EGFR, mainly with L325, and as such any notable hydrogen bonding or packing interactions are not seen. Upon substitution by **pcY**, in both cases, the additional o-nitrobenzyl group protrudes into the binding interface, contacting several EGFR residues. Although initially appearing to be accommodated at the binding interface, as the simulation proceeds, it does not form stable contacts that could compensate for the crowding caused in the region, disrupting binding. On examining Y109, which is also at the binding interface, it is seen to prefer to remain oriented nearly parallel to the EGFR surface throughout the simulation of wt7D12-EGFR complex, interacting significantly with only S418 on EGFR. The 7D12pcY109-EGFR complex simulation demonstrates that the additional o-nitrobenzyl group is accommodated in a large solvent-accessible cleft and does not cause a steric clash with any residue in EGFR allowing the complex to remain bound.

While providing an explanation for the different behavior of Y109 mutant, this study also demonstrates the effectiveness of MD simulations to obtain details about inter-residue interactions in proteins containing unnatural amino acids. The methodology and force field parameters developed here for **pcY** can also be utilized in future studies to predict candidate residues for **pcY** substitution in other proteins.

Light-dependent delivery of fluorophores to live EGFR-positive cancer cells. We designed experiments to examine and provide evidence that photoactive antibodies can mediate light-dependent delivery of small molecules to the surface of live A431 cells. 7D12 and 7D12pcY32 were labeled using N-hydroxysuccinimide (NHS) ester of a fluorophore, BODIPY-TMR-X (Supporting Information). We first assessed if the presence of this label on 7D12 influences 7D12-EGFR binding, using cell-ELISA based experiments. Comparison of unlabeled and labeled 7D12 reveal that the binding is reduced by ~1.5-fold due to the presence of the BODIPY-TMR-X label (Figure S10), hence at least 1.5-fold higher concentration of labeled sample would be required for further experiments. The light-dependent localization of photoactive antibody on the surface of live A431 cells was evaluated using fluorescence microscopy in a dynamic experimental setup. The microscope was fitted with a flow chamber, with the flow rate of media and the labeled antibody fragments fixed at 1 ml/min throughout the experiment. Images were acquired every 30 sec, except during irradiation with 365 nm light. Media was initially passed for 5 min through the chamber containing A431 cells, followed by 500 nM solution of labeled 7D12pcY32 for 2 min, and then again media for 10 min. 30 sec after injecting the labeled 7D12pcY32, a burst of fluorescence was observed, which continued for 2 min during the movement of labeled 7D12pcY32 over the cells. Next, labeled 7D12pcY32 was again passed through the chamber for 2 min, but this time, after 1 min, the chamber was irradiated with 365 nm light for 1 min for decaging **pcY**. Subsequent to an initial burst of fluorescence due to movement of labeled 7D12pcY32, a detectable fluorescence signal was observed even 2 min after stopping the injection of

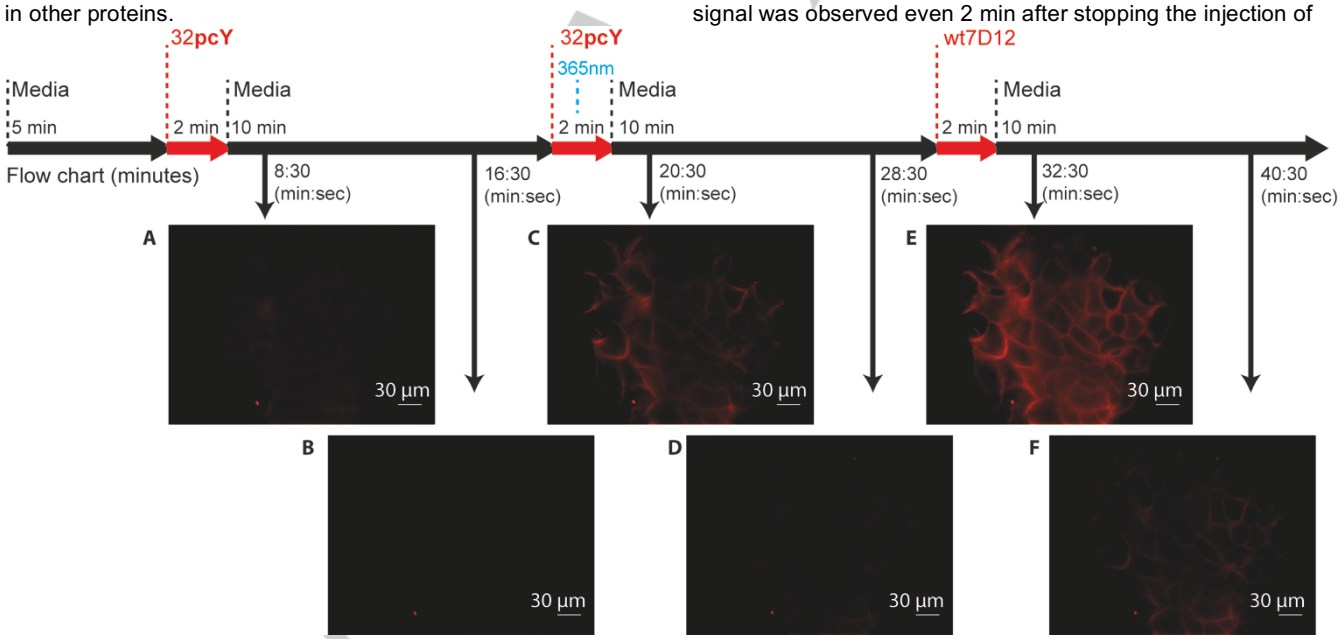

Figure 4. Light-mediated delivery of fluorophores by photoactive antibodies on live A431 cells. (A) Labeled 7D12**pcY**$_{32}$ is injected at 5 min. Near-background fluorescence is observed 1.5 min after passing labeled 7D12**pcY**$_{32}$ over live A431 cells demonstrating that due to the presence of caged group 7D12**pcY**$_{32}$ does not bind to the cell surface. (B) Background fluorescence before re-injecting labeled 7D12**pcY**$_{32}$. (C) Labeled 7D12**pcY**$_{32}$ was injected at 17 min and the irradiated with 365 nm light at 18 min. Significant fluorescence was observed 1.5 min after stopping the injection of labeled 7D12**pcY**$_{32}$, demonstrating light-dependent localization of 7D12 on the surface of A431 cells. (D) Fluorescence from 7D12 reduces to background level presumably due to endocytosis of 7D12 and degradation of the fluorophore. (E) Labeled wt7D12 was injected at 29 min. Significant fluorescence observed 1.5 min after stopping the injection of labeled wt7D12 due to localization of labeled wt7D12 on the surface of A431 cells. (F) Fluorescence from wt7D12 slowly reduces to near background level presumably due to endocytosis of 7D12 and degradation of the fluorophore. See Movie S1 in the supporting information.

labeled 7D12pcY32. Comparison of fluorescence signals observed 1.5 min after stopping the flow of labeled 7D12pcY32 before (Figure 4A) and after (Figure 4C) irradiation, demonstrates light-dependent delivery of fluorophores mediated by 7D12 on the surface of live A431 cells. The fluorescence signal from 7D12 bound to the surface of A431 cells eventually decays to background level, presumably because of endocytosis of 7D12 and degradation of the fluorophore (Figure 4D).

Finally, as a control, 500 nM solution of labeled wt7D12 is passed through the chamber for 2 min and fluorescence signal was observed 1.5 mins after stopping the flow of labelled wt7D12, consistent with receptor-mediated localization of wt7D12 (Figure 4E). The fluorescence signal for wt7D12 is stronger than for decaged 7D12pcY32 (Figure 4C) as the latter flows in the caged form for 1 min and decaged form for 1 min, thus reducing the effective concentration of actively binding 7D12 to half, when compared to wt7D12 that flows for 2 min. Overall, these results are consistent with light-dependent delivery of fluorophores on the surface of EGFR-positive cancer cells.

This study demonstrates that photoactive antibodies can deliver small molecules to specific cancer cells in a light-dependent manner. Extending these antibodies to deliver cytotoxic drugs will provide a highly targeted, light- and receptor-specific approach for cancer therapy.

Conclusion

We report highly efficient genetic site-specific incorporation of unnatural amino acids into antibody fragments expressed in *E. coli*. Replacement of specific tyrosine residues with unnatural photocaged tyrosine in the antigen binding domain of an antibody fragment, 7D12, allowed development of photoactive antibodies. Light-mediated binding of photoactive antibodies to their target, EGFR, was demonstrated using a robust and simple assay performed on the cell surface. Computational methods were used to study the dynamics of 7D12-EGFR interaction and explain the effect of the photocaging group when placed at different sites in the 7D12-EGFR binding interface. Finally, we show in a dynamic experiment that photoactive antibodies can deliver small molecules to the surface of live cancer cells in a light-dependent manner.

The photoactive antibody fragments developed in this report have a molecular weight difference of less than 1% from their original counterparts. Introducing similar modifications in currently used therapeutic antibodies will have direct application for treatment of skin carcinomas, where antibody could be activated by 365 nm light. Activation of photoactive antibodies by more penetrating long wavelength light can be assisted by using upconverting nanoparticles[26] or two-photon activation.[27] Photoactive antibodies would also be useful for treatment of solid tumors in other body parts, where photoactivation can be achieved by surgically implanted biocompatible light emitting diodes (LEDs).[28]

Experimental Section

Expression of wt7D12, 7D12pcY32, 7D12pcY109, and 7D12pcY113. Chemically competent BL21(DE3)pLysS cells containing pULTRA_*Mj*pcYRS/*Mj*tRNA$_{CUA}$ plasmid were transformed with pSANG10_7D12 plasmid or its amber mutants. The cells were recovered by incubating in 1 ml SOB medium at 37°C for 1h. 50 µl of recovered cells were transferred on LB agar plate supplemented with 50 µg ml^{-1} of kanamycin and 75 µg ml^{-1} of spectinomycin. The plates were incubated at 37°C for 12-16 hrs. A single colony from each plate was used for inoculation of 50 ml of 2xTY-GKS media (2xTY media supplemented with 4% glucose, 50 µg ml^{-1} kanamycin and 75 µg ml^{-1} of spectinomycin) and incubated overnight (12-16 h) at 37°C, 220 rpm. The overnight culture was diluted to OD600= 0.1 and incubated until the OD600 reached 0.4-0.6 (37°C, 220rpm, 2-3 h). Once the desired growth was reached, the culture was induced with IPTG (1 mM final concentration) and supplemented with **pcY** (4 mM final concentration) for expression with unnatural amino acids. The culture was incubated overnight (30°C, 160 rpm, 12-16 h). Cells were pelleted (3200g, 4°C, 10 min) and periplasmic extraction was performed using a previously reported procedure.[29] After periplasmic extraction, the protein was purified via its C-terminus hexa-histidine tag using Ni-NTA resin. Subsequently, the samples were concentrated using Vivaspin 500 columns with 3 kDa molecular weight cut-off (GE Healthcare) and the yields were determined using a calorimetric Pierce BCA protein assay (ThermoFisher Scientific) measured at 562 nm. All protein samples were analysed using SDS-PAGE. Samples were heated with Nu-PAGE LDS loading buffer (Invitrogen) at 95°C for 15 min, centrifuged at 13,000g for 15 min at 4°C and loaded on 4-12% Bis-Tris gel (Invitrogen) along with BIO-RAD pre-stained protein ladder (Precision Plus All Blue Protein Standards) as a marker. The gel was stained with Coomassie Blue (InstantBlue, Expedeon). The identity of protein samples was further confirmed using electrospray ionization mass spectrometry coupled with liquid chromatography (LC-MS).

On-cell assay for measuring the binding of His-tagged antibody fragments. A-431 and MDA-MB-231 cells were grown in a T-75 flask in complete medium (DMEM, 10% FBS, 1% PEN/STREP) using standard tissue culture procedures until 80-90% confluence. After washing with 1x phosphate buffered saline (PBS) and trypsinising, cells were pelleted (300g, 5 minutes) and resuspended in 10 ml fresh complete medium. The cells were then counted on a hemocytometer and diluted to 200,000 cells/ml. 200 µl of this solution was dispensed into each well (40,000 cells/well) of a 96-well plate and grown overnight until 80-90% confluence. Once the desired confluence was reached, medium was replaced with 200 µl of complete medium supplemented with 7D12 or its photocaged mutants at the desired concentration. The plate was incubated for 10 minutes (37°C, 5% CO2). After removing medium, the cells were fixed using formaldehyde. 150 µl of 3.7% formaldehyde solution in 1xPBS was added to each well and incubated for 20 min at room temperature. The formaldehyde solution was removed and cells were washed three times (200 µl, 5 minutes, gentle rocking) with PBST (1X PBS supplemented with 1% Tween-20). After removing the wash buffer, 100 µl of blocking buffer (10% milk in PBST) was added and cells were incubated at room temperature for 1 h with gentle rocking. The blocking buffer was removed. 50 µl solution containing primary anti-6x-His tag antibody was added to each well and the plate was incubated at room temperature for 1 h. The primary antibody solution contained mouse anti-6x-His tag antibody (ThermoFisher Scientific) at 1:500 dilution and 1% milk in PBST. After incubation with the primary antibody, cells in each well were washed three times with PBST (200 µl, 5 minutes, gentle rocking). Subsequently, 50 µl of HRP-linked secondary antibody solution was applied to each well and incubated at room temperature for 1 h. The HRP-linked secondary antibody solution contained anti-mouse-HRP-linked antibody (Cell Signaling) at 1:1000 dilution and 1% milk in PBST. After incubation with secondary antibody, the cells were washed five times with PBST (200 µl, 5 minutes, gentle rocking). Finally, 200 µl of SuperSignal chemiluminescent Substrate (ThermoFisher Scientific) was added to each well and the plate was imaged using BIORAD GelDoc XR+. The plate was further quantified by

measuring chemiluminescence signal using a CLARIOstar plate reader (BMG labtech).

Acknowledgements

We thank Prof. Nick Le Brun and Dr. Jason C. Crack for help with ESI-MS experiments, and Prof. Jason Chin for sharing plasmids. We also thank Prof. Peter G. Schultz, Prof. Shankar Balasubramanian and Prof. John McCafferty for sharing plasmids with Addgene and thank Addgene for providing the plasmids. This work was partly funded by the Wellcome trust (204593/Z/16/Z).

Keywords: Unnatural amino acids • Light-activated • Photocaged Tyrosine • Antibodies • Cancer

[1] a) S. Kassem, T. van Leeuwen, A. S. Lubbe, M. R. Wilson, B. L. Feringa, D. A. Leigh, *Chem. Soc. Rev.* **2017**, *46*, 2592-2621; b) C. Cheng, J. F. Stoddart, *Chemphyschem* **2016**, *17*, 1780-1793; c) S. Ranallo, C. Prevost-Tremblay, A. Idili, A. Vallee-Belisle, F. Ricci, *Nat. Commun.* **2017**, *8*, 15150; d) C. Chou, D. D. Young, A. Deiters, *Angew. Chem. Int. Ed. Engl.* **2009**, *48*, 5950-5953.

[2] a) S. M. Douglas, I. Bachelet, G. M. Church, *Science* **2012**, *335*, 831-834; b) J. Broichhagen, M. Schonberger, S. C. Cork, J. A. Frank, P. Marchetti, M. Bugliani, A. M. Shapiro, S. Trapp, G. A. Rutter, D. J. Hodson, D. Trauner, *Nat. Commun.* **2014**, *5*, 5116; c) S. Erbas-Cakmak, D. A. Leigh, C. T. McTernan, A. L. Nussbaumer, *Chem. Rev.* **2015**, *115*, 10081-10206.

[3] a) Y. S. Chen, M. Y. Hong, G. S. Huang, *Nat. Nanotechnol.* **2012**, *7*, 197-203; b) G. J. Weiner, *Nat. Rev. Cancer* **2015**, *15*, 361-370.

[4] L. R. Desnoyers, O. Vasiljeva, J. H. Richardson, A. Yang, E. E. Menendez, T. W. Liang, C. Wong, P. H. Bessette, K. Kamath, S. J. Moore, J. G. Sagert, D. R. Hostetter, F. Han, J. Gee, J. Flandez, K. Markham, M. Nguyen, M. Krimm, K. R. Wong, S. Liu, P. S. Daugherty, J. W. West, H. B. Lowman, *Sci. Transl. Med.* **2013**, *5*, 207ra144.

[5] S. B. Gunnoo, H. M. Finney, T. S. Baker, A. D. Lawson, D. C. Anthony, B. G. Davis, *Nat. Commun.* **2014**, *5*, 4388.

[6] a) B. S. Howerton, D. K. Heidary, E. C. Glazer, *J. Am. Chem. Soc.* **2012**, *134*, 8324-8327; b) F. Reessing, W. Szymanski, *Curr. Med. Chem.* **2017**, *24*, 4905-4950.

[7] A. M. Scott, J. D. Wolchok, L. J. Old, *Nat Rev Cancer* **2012**, *12*, 278-287.

[8] T. T. Hansel, H. Kropshofer, T. Singer, J. A. Mitchell, A. J. George, *Nat. Rev. Drug Discov.* **2010**, *9*, 325-338.

[9] M. Mitsunaga, M. Ogawa, N. Kosaka, L. T. Rosenblum, P. L. Choyke, H. Kobayashi, *Nat. Med.* **2011**, *17*, 1685-1691.

[10] J. Hemphill, C. Chou, J. W. Chin, A. Deiters, *J. Am. Chem. Soc.* **2013**, *135*, 13433-13439.

[11] A. Gautier, A. Deiters, J. W. Chin, *J. Am. Chem. Soc.* **2011**, *133*, 2124-2127.

[12] D. P. Nguyen, M. Mahesh, S. J. Elsasser, S. M. Hancock, C. Uttamapinant, J. W. Chin, *J. Am. Chem. Soc.* **2014**, *136*, 2240-2243.

[13] J. K. Bocker, W. Dorner, H. D. Mootz, *Chem. Commun. (Camb)* **2019**, *55*, 1287-1290.

[14] a) N. Normanno, A. De Luca, C. Bianco, L. Strizzi, M. Mancino, M. R. Maiello, A. Carotenuto, G. De Feo, F. Caponigro, D. S. Salomon, *Gene* **2006**, *366*, 2-16; b) S. Li, K. R. Schmitz, P. D. Jeffrey, J. J. Wiltzius, P. Kussie, K. M. Ferguson, *Cancer Cell* **2005**, *7*, 301-311.

[15] a) N. E. Hynes, H. A. Lane, *Nat. Rev. Cancer* **2005**, *5*, 341-354; b) R. Perez-Soler, L. Saltz, *J. Clin. Oncol.* **2005**, *23*, 5235-5246.

[16] S. Muyldermans, *Annu. Rev. Biochem.* **2013**, *82*, 775-797.

[17] a) R. C. Roovers, T. Laeremans, L. Huang, S. De Taeye, A. J. Verkleij, H. Revets, H. J. de Haard, P. M. van Bergen en Henegouwen, *Cancer Immunol. Immunother.* **2007**, *56*, 303-317; b) R. C. Roovers, M. J. Vosjan, T. Laeremans, R. el Khoulati, R. C. de Bruin, K. M. Ferguson, A. J. Verkleij, G. A. van Dongen, P. M. van Bergen en Henegouwen, *Int. J. Cancer* **2011**, *129*, 2013-2024.

[18] a) G. Biffi, D. Tannahill, J. McCafferty, S. Balasubramanian, *Nat. Chem.* **2013**, *5*, 182-186; b) C. D. Martin, G. Rojas, J. N. Mitchell, K. J. Vincent, J. Wu, J. McCafferty, D. J. Schofield, *BMC Biotechnol.* **2006**, *6*, 46.

[19] a) A. Deiters, D. Groff, Y. Ryu, J. Xie, P. G. Schultz, *Angew. Chem. Int. Ed. Engl.* **2006**, *45*, 2728-2731; b) E. Arbely, J. Torres-Kolbus, A. Deiters, J. W. Chin, *J. Am. Chem. Soc.* **2012**, *134*, 11912-11915.

[20] a) A. Chatterjee, S. B. Sun, J. L. Furman, H. Xiao, P. G. Schultz, *Biochemistry* **2013**, *52*, 1828-1837; b) A. Sachdeva, K. Wang, T. Elliott, J. W. Chin, *J. Am. Chem. Soc.* **2014**, *136*, 7785-7788.

[21] K. R. Schmitz, A. Bagchi, R. C. Roovers, P. M. van Bergen en Henegouwen, K. M. Ferguson, *Structure* **2013**, *21*, 1214-1224.

[22] R. Railkar, L. S. Krane, Q. Q. Li, T. Sanford, M. R. Siddiqui, D. Haines, S. Vourganti, S. J. Brancato, P. L. Choyke, H. Kobayashi, P. K. Agarwal, *Mol. Cancer Ther.* **2017**, *16*, 2201-2214.

[23] a) W. Jiang, S. Cossey, J. N. Rosenberg, G. A. Oyler, B. J. Olson, D. P. Weeks, *BMC Plant Biol.* **2014**, *14*, 244; b) B. P. Delisle, H. A. Underkofler, B. M. Moungey, J. K. Slind, J. A. Kilby, J. M. Best, J. D. Foell, R. C. Balijepalli, T. J. Kamp, C. T. January, *J. Biol. Chem.* **2009**, *284*, 2844-2853.

[24] S. Spinelli, L. G. Frenken, P. Hermans, T. Verrips, K. Brown, M. Tegoni, C. Cambillau, *Biochemistry* **2000**, *39*, 1217-1222.

[25] J. C. Phillips, R. Braun, W. Wang, J. Gumbart, E. Tajkhorshid, E. Villa, C. Chipot, R. D. Skeel, L. Kale, K. Schulten, *J. Comput. Chem.* **2005**, *26*, 1781-1802.

[26] S. Wen, J. Zhou, K. Zheng, A. Bednarkiewicz, X. Liu, D. Jin, *Nat. Commun.* **2018**, *9*, 2415.

[27] J. Croissant, M. Maynadier, A. Gallud, H. Peindy N'dongo, J. L. Nyalosaso, G. Derrien, C. Charnay, J. O. Durand, L. Raehm, F. Serein-Spirau, N. Cheminet, T. Jarrosson, O. Mongin, M. Blanchard-Desce, M. Gary-Bobo, M. Garcia, J. Lu, F. Tamanoi, D. Tarn, T. M. Guardado-Alvarez, J. I. Zink, *Angew. Chem. Int. Ed. Engl.* **2013**, *52*, 13813-13817.

[28] H. Zhang, J. A. Rogers, *Adv. Opt. Mater.* **2019**, *7*, 1800936-1800936.

[29] R. Rouet, D. Lowe, K. Dudgeon, B. Roome, P. Schofield, D. Langley, J. Andrews, P. Whitfeld, L. Jermutus, D. Christ, *Nat. Protoc.* **2012**, *7*, 364-373.

Entry for the Table of Contents (Please choose one layout)

Layout 1:

RESEARCH ARTICLE

Text for Table of Contents

((Insert TOC Graphic here))

*Author(s), Corresponding Author(s)**

Page No. – Page No.

Title

Layout 2:

RESEARCH ARTICLE

((Insert TOC Graphic here))

*Author(s), Corresponding Author(s)**

Page No. – Page No.

Title

Text for Table of Contents